*Journal of Global Positioning Systems*

# Effects of Signal Deformations on Modernized GNSS Signals

**R. Eric Phelts**

Department of Aeronautics and Astronautics,
*Stanford University*, 496 Lomita Mall, Room 250 Stanford, CA 94305
Email: pheltsre@stanford.edu

**Dennis M. Akos**

*University of Colorado*
429 UCB Aerospace Engineering Sciences,
University of Colorado, Boulder, CO 80309-0429
Email: dma@colorado.edu

Received: / Accepted:

**Abstract**. Satellite-based navigation requires precise knowledge of the structure of the transmitted signals. For GPS, accurate knowledge of the shape of the code correlation peaks is required to ensure no biases are introduced into the position solution. It is generally presumed that all GPS-like satellite signals are virtually identical. However, in 1993 a satellite malfunction introduced significant distortion onto one of the satellite C/A codes. That distortion caused range errors to vary with receiver filter characteristics and code tracking loop implementation. As a result, high-integrity systems such as the Wide Area Augmentation System (WAAS) must implement signal deformation monitors to detect and remove signals that become anomalously distorted.

In the future, WAAS will rely on modernized signals from both GPS (L5) and Galileo (E1/L1/E2 and E5A/E5B). This should increase performance for users; however they must still protect against potential signal deformations. Although the International Civil Aviation Organization (ICAO) has agreed on a threat scenario for GPS L1 signals, no such agreement exists for modernized signals. In addition, each of these signals will have different chipping rates and their correlation peak structures will be quite different from that of the GPS C/A code. Their code tracking loop implantations are as yet not well-defined, but may differ somewhat from traditional architectures. An additional complication is the unknown receiver filter characteristics that the new receivers will employ. Each of these factors may render a given signal and/or receiver configuration more or less sensitive to signal deformations.

This paper analyzes the range error sensitivity of several modernized signals subjected to distortions of the type considered in the ICAO threat model for signal deformations. To isolate the effects of the signal-in-space deformation errors, it assumes an ideal, wideband receiver filter and basic early-minus-late code tracking implementations for the new codes. It also compares the distortion-induced range errors for the new codes to those currently modeled for the C/A code. Finally, these results are used to motivate threat model refinements and receiver tracking loop constraints that minimize the affects of this error source for the modernized GNSS signals.

**Key words:** SV19, signal distortion, signal deformation, signal quality monitoring, satellite failures

## 1 Introduction

### 1.1 SV19

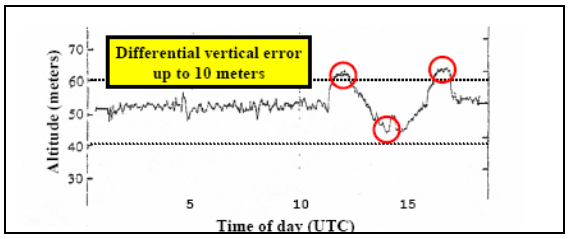


**Fig. 1 Differential vertical position errors due to SV19 as measured by Trimble Navigation, Ltd in March of 1993.**

SV19 was launched on October 21, 1989 and declared operational in November of the same year. In March 1993 at the Oskosh Air Show, Trimble Navigation, Ltd. noted that differential position accuracies, based on code pseudorange measurements, were less than 50 cm when not using SV19. When SV19 was included, the vertical position accuracy of the differential code phase solution degraded to anywhere from 3 to 10 meters. (See Figure 1.) Also, at Camp Parks Reserve Forces Training Area in Pleasanton, CA, the C/A code was directly measured using an oscilloscope in series with a high-gain antenna. (See Fig. ) It revealed a misalignment in the transitions of the C/A. The problem was resolved in January 2004 when the Operational Control Segment commanded the satellite to use onboard redundant signal transmission hardware. (Edgar, et al, 2000)

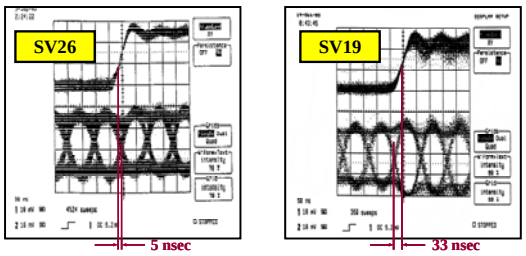


**Fig. 2 [LEFT] C/A code edges on healthy SV aligned to equipment measurement accuracy—within 3-6ns; [RIGHT] C/A code edges on SV19 misaligned by approximately 28-33ns with respect to P(Y)-code edges.**

### 1.2 ICAO Threat Model for Signal Deformations:

Several candidate threat models—spanning the range from very simple models to very complex—were initially proposed to explain the SV19 event (Enge et al, 1999). Such threats manifest themselves in the form of an anomalous correlation peak. Accordingly, each of the following may result in uncorrected error for a differential GPS (DGPS) user with a receiver configuration that differs from that of the reference station:

- Dead zones: "Flat spots," or plateaus atop the correlation peak, are regions of zero discriminator gain. The airborne and reference receiver correlator pairs may "track" in different portions of this region.
- Distortions: Asymmetries caused by underdamped oscillations in the correlation function may affect the airborne receivers differently than the reference station. Even using multiple correlators, monitor receivers may not detect these distortions.
- False peaks: Significant distortion of the correlation peak may cause some receivers to lock onto (i.e., track) the distorted or evil waveform (EWF)-induced peak—a raised oscillation—instead of the true one.

A "2nd-Order Step" based model was developed to address these three correlation peak pathologies. It was adopted by the International Civilian Aviation Organization (ICAO) in May of 2000 as the standard method for modeling anomalous signal deformation. This threat model is capable of generating deadzones, distortions, and false peaks on the receiver correlation peak. It fits well with observations and provides plausible explanations the measured code distortion and nearly 10 meter differential vertical position errors. It uses only three parameters and is accordingly relatively simple to simulate and test. In addition, this model generates causal waveforms, which are more plausible candidates for future failure modes of the real satellite signal generating hardware.

As illustrated in Fig. , the ICAO threat model approximates three specific classes of failure modes: digital, analog, and combination (analog and digital) failure modes. This model assumes the anomalous waveform is some combination of second-order ringing (an analog failure mode) and lead/lag (a digital failure mode) of the pseudorandom noise code chips. The model includes parameter bounds for $F_d$ (damped natural frequency), $\sigma$ (damping), and $\Delta$ (lead/lag). An effective ground signal quality monitoring (SQM) implementation—such as the ones envisioned for Wide Area Augmentation Systems (WAAS)—would detect any and all such deformations that would result in unacceptably large DGPS pseudorange errors. (Phelts, 2001)

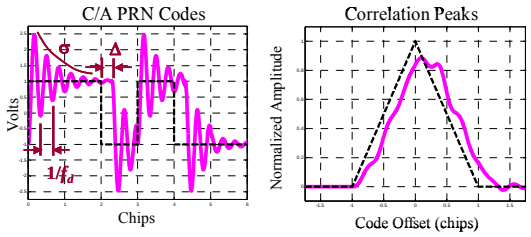


**Fig. 3 Combination of Analog ($F_d$ and σ) and Digital (Δ) Failure Modes (Ideal <dashed> and Evil <solid> Waveforms Shown.)**

Signal deformation threat models specific to each of the modernized signals have not been defined as yet. However, the ICAO threat model provides a good starting point for these investigations. The aforementioned peak pathologies characterize a wide variety of deformations about which WAAS is concerned. The bounds used to limit the ICAO threat model parameters (Phelts et al, 2000) may not necessarily apply. Still, preliminary analyses of robustness against these threats and tracking design constraints can begin to be made by applying these (and other) parameter values to the envisioned codes. The results should provide some insights into practical threat model bounds and system receiver design constraints.

## 2 Analysis

### 2.1 Mathematical Models of Signals

The analysis of this paper assumes the incoming signals have been translated to baseband and are phase locked with zero phase error. To model a BOC(*n,m*) code at a chipping rate of *m**1.023MHz, the following equation may be used

$$c_{n,m}(t) = c_{\mathrm{m}}(t) \cdot \mathrm{s}_{\mathrm{n}}(t) \tag{1}$$

where $\mathrm{s}_{\mathrm{n}}(t)$ is a square wave of frequency *n**1.023MHz. For this paper, the GPS PRN1 was used for $c_{\mathrm{m}}(t)$. A square wave was then modulated onto it at a frequency of *n**1.023MHz.

Code distortion may be analyzed by examining the autocorrelation functions. The ideal autocorrelation function ${}_{n,m}R(\tau)$ is given by

$${}_{n,m}R(\tau) = \int_{-\infty}^{\infty} {}_{n,m}H(f)\,{}_{n,m}C(f)\,{}_{n,m}C_R^*(f)e^{j2\pi f}\,df \tag{2}$$

where, ${}_{n,m}H(f)$ represents the transfer function of the combined filter that affect the incoming signal $C(f)$. For accurate modeling, ${}_{n,m}H(f)$ should include the filters on the satellite, the antenna and LNA, and inside the receiver. $C_R^*(f)$ is the complex conjugate of the power spectrum of the replica code.

#### 2.1.1 Correlation Peak Distortion models

A digital lead/lag distortion can be modeled as a circular shift of a single code sequence added/subtracted from a standard code sequence. A general equation for modeling lead or lag distortions is given below

$${}_{n,m}c_{\Delta}(t) = \begin{cases} \max\left[\left({}_{n,m}c(t+\Delta) - {}_{n.m}c(t)\right), 0\right], & \Delta \le 0 \\ \min\left[\left({}_{n,m}c(t+\Delta) - {}_{n.m}c(t)\right), 0\right], & \textit{otherwise} \end{cases} \tag{3}$$

$${}_{n,m}c_{d(\Delta)}(t) = {}_{n,m}c(t) + {}_{n,m}c_{\Delta}(t) \tag{4}$$

It follows that a correlation peak distorted by this failure mode is found from

$${}_{n,m}R_{d(\Delta)}(\tau) = \int_{-\infty}^{\infty} {}_{n,m}H(f)\,{}_{n,m}C_{d(\Delta)}(f)\,{}_{n,m}C_R^*(f)e^{j2\pi f}\,df \tag{5}$$

Where ${}_{n,m}C_{d(\Delta)}$ is the frequency domain representation of the digitally-distorted code ${}_{n,m}c_{d(\Delta)}(t)$.

The transfer function of the 2nd-order filter for representing the analog failure mode is given by

$$H_d(s) = \frac{(\omega_0)^2}{s^2 + 2\zeta\omega_0 s + (\omega_0)^2} \tag{6}$$

Where $\sigma = \zeta\omega_0$ (the product of the damping ratio $\zeta$ and the natural frequency $\omega_0$) and is defined as the damping/attenuation factor, σ in MNepers/sec.

and is defined as the damping/attenuation factor,σ in MNepers/sec.

And the damped frequency of oscillation, $F_d$, is found from

$$F_d = \frac{1}{2\pi}\sqrt{1-\zeta^2} \tag{7}$$

Using this filter to modify the incoming signal yields the following expression for the deformed correlation peak

$${}_{n,m}R_{d(fd,\sigma)}(\tau) = \int_{-\infty}^{\infty} H_d(f)\,{}_{n.m}H(f)\,{}_{n.m}C(f)\,{}_{n.m}C_R^*(f)e^{j2\pi f}\,df \tag{8}$$

where we have substituted s = σ+2πjf, into $H_d(s)$ to produce $H_d(f)$ as the frequency domain representation of the 2nd-order response filter function.

The equation for the correlation function of a signal affected by both analog and digital failure modes is provided below. An exploration of the errors resulting from this combination failure mode is beyond the scope of this paper

$$ {}_{n,m}R_{d(fd,\sigma,\Delta)}(\tau) = \int_{-\infty}^{\infty} H_d(f)_{n,m}H(f)_{n,m}C_{d(\Delta)}(f)_{n,m}C_R^*(f)e^{j2\pi f}df \quad (9)$$

### 2.1.2 Satellite and Receiver Filter models

For this paper only infinite bandwidth, ideal "brick wall" rectangular filters were modeled. The center frequencies ($f_c$) and bandwidths of these filters are found according to the respective ICD specifications of the following full-bandwidth signals: GPS C/A code, GPS-L5, and Galileo.

All of the current and envisioned GNSS signals except for the E5a/b signal were filtered using a rectangular filter of magnitude 0dB for $f_c$-20≤$bw$≤ $f_c$+20 and -200dB otherwise. The E5a/b signal for Galileo, however, is a BOC(15,10) code and is 90MHz wide. The first filter applied to it had a magnitude of 0dB for $({}_{n,m}f_c)$-45≤$bw$≤$({}_{n,m}f_c)$+45 and -200dB otherwise. To single out the E5a signal a secondary filter was applied at a frequency offset of $({}_{15,10}f_c)$-22.5*1.023MHz and a bandwidth of 45MHz was also applied. The transition band attenuation for this filter was 30dB per octave. For simplicity, no group delay effects were modeled in this analysis; however, this is an added design variable that will need to be included in more comprehensive investigations.

### 2.1.3 Tracking error models

Assuming coherent tracking and negligible phase error, the steady-state tracking error for an early-minus-late discriminator about the equilibrium point is given by equation 11 below.

$$ {}_{n,m}\tau = \arg\left[ {}_{n,m}R_{d(\bullet)}\left(\tau - \frac{d}{2}\right) - {}_{n.m}R_{d(\bullet)}\left(\tau + \frac{d}{2}\right) = 0 \right] \quad (11)$$

A comparison of how this discriminator compares to other implementations is not included in this paper.

### 2.2 Summary of Assumptions

The tracking error biases for correlator spacings relative to an ideal, undistorted correlation peak were modeled. No measurement noise or multipath errors were considered. (Correlator spacings will be given in chips, where the chip size, is determined by the chipping rate $m$.)

Only standard early-minus late tracking was analyzed, and the carrier loop was assumed to be phase-locked and have zero phase error.

*Digital Failure mode*: The range of this failure was modeled to be between 0 to 0.12 microseconds—the maximum extent of the ICAO threat model for GPS C/A code—in increments of 0.01 microseconds. For the Galileo codes, the deformation was assumed to occur on the square wave generator(s) only. It is later demonstrated that larger errors may occur if both code and square wave modulators are both assumed to be distorted; a smaller tracking errors can be observed if only the code modulator is affected. Note that for Galileo or GPS codes with $m$≥1-chip, lead/lag distortion may precipitate excessive bit-errors or perhaps a loss of continuous tracking in an actual receiver. Alternatively, it may simply result in multiple peaks, so this possible threat limitation was not considered in this analysis.

*Analog failure mode:* This failure was modeled for each code type using a single (example) correlator spacing. The range of the damped frequency parameter was 1≤$F_d$≤50MHz in 1MHz increments. The current ICAO threat model extends, at most, to 17MHz (single-sided bandwidth) for this failure mode. The attenuation parameter was assumed to vary according to 0.1≤$\sigma$≤10MNepers/sec in increments of 1MNep/s. The ICAO threat model for GPS C/A code uses 0.8≤σ≤8.8MNepers/sec.)

## 3 Results

Each of the following GPS and assumed Galileo code autocorrelations were modeled for the digital-only and analog-only failure modes:

- C/A Code BPSK or BOC(0,1) centered on 1575.42MHz; 40MHz bandwidth
- L5 and P(Y) code: BPSK or BOC(0,10) centered on 1176.45 ; 40MHz bandwidth
- E5A/E5B: 2 x NPSK (10.23 Mcps) or BOC (15,10) between 1164-1215 MHz
- E6: BPSK (5.115 Mcps) & BOC (10,5) centered at ~1279 MHz (1260-1300 MHz)
- BOC (1,1) Open Service (OS)
- BOC (15,2.5) cosine phased Public Regulated Service (PRS)

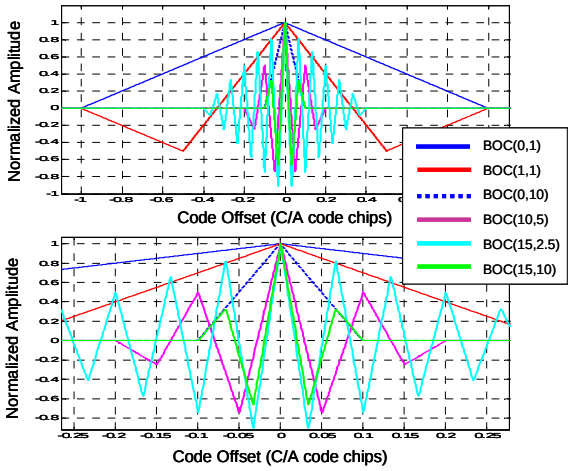


**Fig. 4 Six BOC(n,m) correlation peaks plotted relative to BOC(0,1)—C/A code**

The nominal autocorrelation peaks for each of the six types are shown in Figure 4. For comparison, they are each plotted as a function of C/A code chip offset.

### 3.1 Digital Distortion

Figures 5 through 7 contrast the nominal and deformed peaks with a $\Delta$=0.1μsec for each of the following code modulations: BOC(0,1) and BOC(1,1); BOC(0,10) and BOC(10,5); BOC(15,2.5) and BOC(15,10), respectively. Each plot normalizes the correlation peak offsets (x-axis) by the chipping rate. (Relative to Figure 4, each peak appears *m* times as wide.)

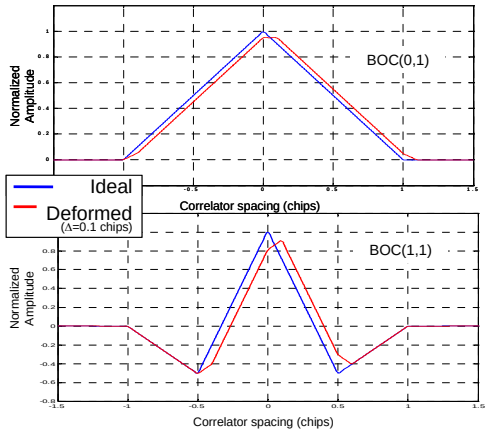


**Fig. 5 Digital distortion of +0.1μsec plotted for BOC(0,1) [top] and BOC(1,1) [bottom]**

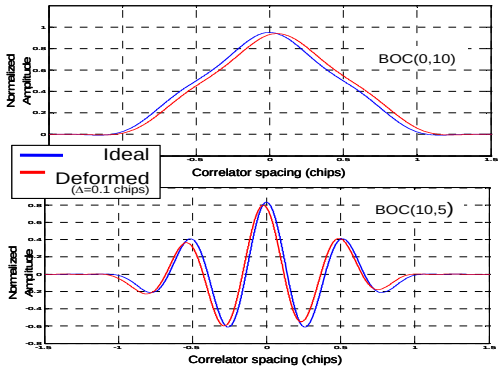


**Fig. 6 Digital distortion of +0.1μsec plotted for BOC(0,10) [top] and BOC(10,5) [bottom]**

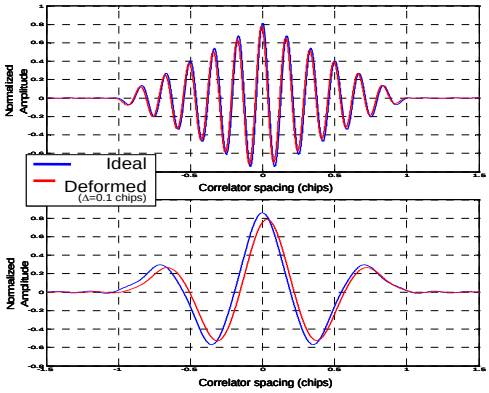


**Fig. 7 Digital distortion of +0.1μsec plotted for BOC(15,2.5) [top] and BOC(15,10) [bottom]**

Figures 8 through 15 show the tracking errors for the codes subjected to digital failure mode and $0 \le \Delta \le 0.12$ μsec. The two-dimensional contours plot tracking errors as a function of $\Delta$ and correlator spacing (normalized by *m*). Figures 10, 11, and 12 show the errors for BOC(1,1) code subjected to a square wave generator (only) lag, both code and square wave generator lag, and a code generator (only) lag failure.

Because the digital deformation primarily causes a shift of the correlation peak (rather than inducing asymmetries) the errors vary more as a function of increasing $\Delta$ than correlator spacing. Previous research has shown that some $\Delta$ is present even on the exiting GPS signals (Mitelman, 2005; Brenner et al, 2002). The smaller correlator spacings and values of $\Delta$, these plots give an indication of typical errors that may be inescapable for these signals. Note, however, for several code incarnations, the correlator spacings plotted may be infeasible. In addition, for some codes, it may be determined that some large digital distortions may be unrealistic failures to model. Because no practical threat bounds have yet been determined for all the future signals, these plots intentionally display results for

parameter values of Δ that extend over a wide range of possible values.

The BOC(0,1), or C/A code, in general, gives the second largest errors (in meters) for most correlator spacings with a maximum of more than 15 meters. The BOC(1,1) (Galileo Open Service code) gives the largest (>30m) since its main peak never fully flattens. The higher-frequency signals all have substantially smaller maximum errors. For practical correlator spacings, the maximum errors are comparable for BOC(0,10) and the other BOC(*n*,*m*) signals where *n*,*m*≠1.

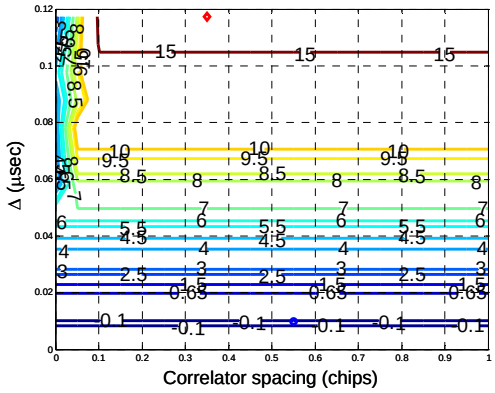


**Fig. 8 BOC(0,1) – Digital (square wave generator) failure-induced range biases (meters)**

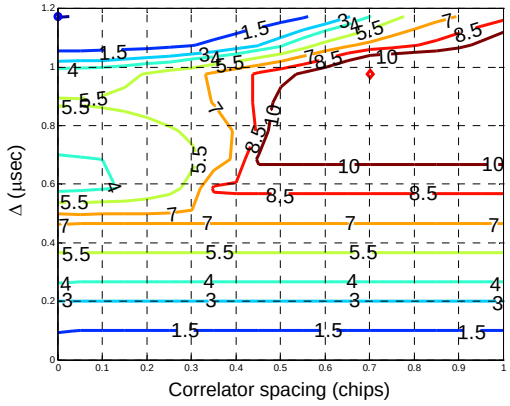


**Fig. 9 BOC(0,10) – Digital (square wave generator) failure-induced range biases (meters)**

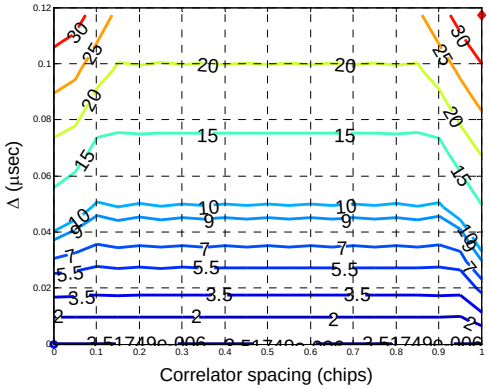


**Fig. 10 BOC(1,1) – Digital (square wave generator) failure-induced range biases (meters)**

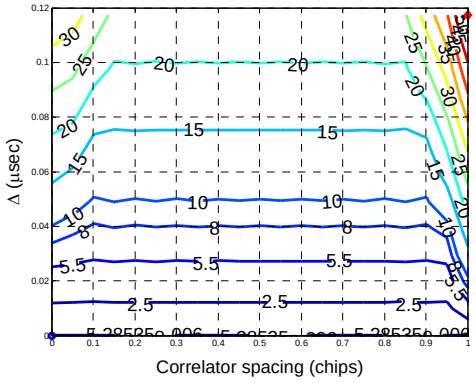


**Fig. 11 BOC(1,1) Digital (square and code generator) failure-induced range biases (meters)**

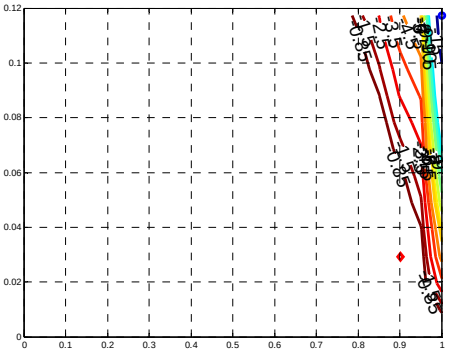

**Fig. 12 BOC(1,1) – Digital (code generator) failure-induced range biases (meters)**

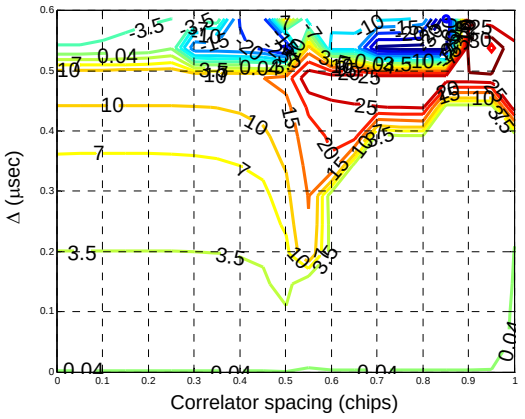


**Fig. 13 BOC(10,5) – Digital (square wave generator) failure-induced range biases (meters)**

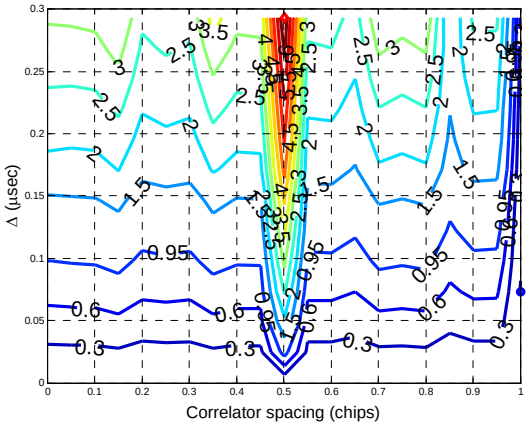


**Fig. 14 BOC(15,2.5) – Digital (square wave generator) failure-induced range biases (meters)**

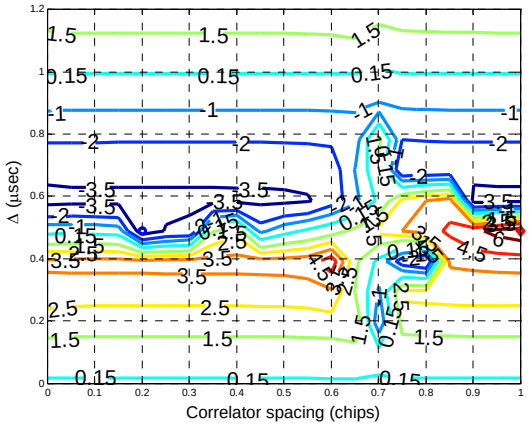


**Fig. 15 BOC(15,10) – Digital (square wave generator) failure-induced range biases (meters)**

### 3.1 Analog Distortion

Figures 16 through 18 contrast the nominal and deformed peaks with a $F_d$=17MHz and σ=8.8MNepers/sec for each of the following code modulations: BOC(0,1) and BOC(1,1); BOC(0,10) and BOC(10,5); BOC(15,2.5) and BOC(15,10), respectively. Each plot normalizes the correlation peak offsets (x-axis) by the chipping rate. (Relative to Figure 4, each peak appears *m* times as wide.)

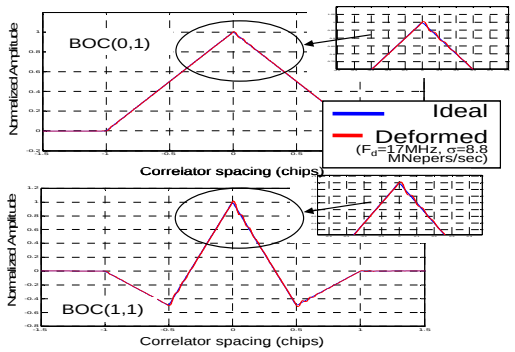


**Fig. 16 Analog distortion with $F_d$=17MHz and σ=8.8MNepers/sec plotted for BOC(0,1) [top] and BOC(1,1) [bottom]**

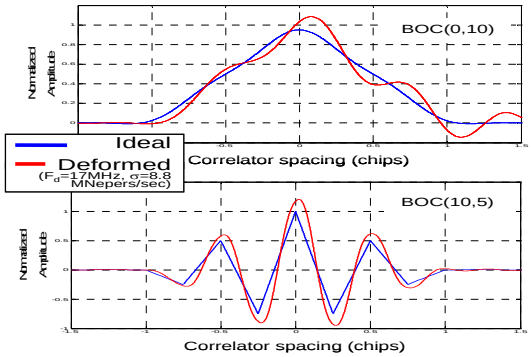


**Fig. 17 Analog distortion with $F_d$=17MHz and σ=8.8MNepers/sec plotted for BOC(0,10) [top] and BOC(10,5) [bottom]**

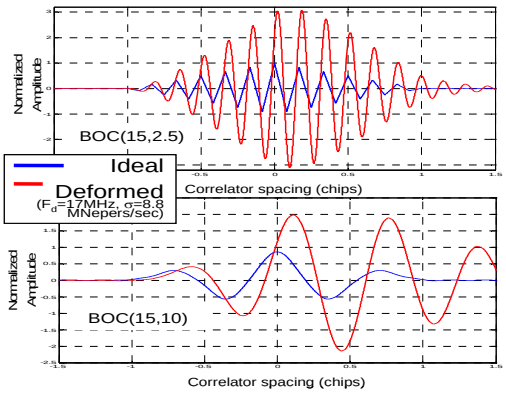


**Fig. 18 Analog distortion with $F_d$=17MHz and σ=8.8MNepers/sec plotted for BOC(15,2.5) [top] and BOC(15,10) [bottom]**

Figures 19 through 24 show the tracking errors for the codes subjected to the analog failure mode and $1 \leq F_d \leq 50$MHz and $0.1 \leq \sigma \leq 10$MNepers/sec. The two-dimensional contours plot tracking errors as a function of $F_d$ and $\sigma$ for a code-specific, example correlator spacing (normalized by $m$) indicated on the plot.

The analog deformation primarily causes correlation peak asymmetry. As a result, these errors will vary significantly as a function of correlator spacing. For any given correlator spacing, the errors vary primarily as a function of $F_d$. As with the digital failure, previous research has shown that some second-order ringing is also present even on the exiting GPS signals (Mitelman, 2005). (Any filtering of the signals will cause some small, nominal analog distortion.)

Also as was true for the digital failure mode, for several future code modulations, it may be determined that some large digital distortions may be unrealistic failures. Because no practical threat bounds have been determined, these plots intentionally display results for parameter values of $F_d$ and $\sigma$ that extend over a wide range of possible values.

Since the correlator spacings differ for each example plotted here, definitive comparisons across BOC code types is difficult. The BOC(0,1) (or C/A code), in general, gives the largest errors; however it is only valid for the ICAO threat range of $4 \leq F_d \leq 17$MHz and $0.8 \leq \sigma \leq 8.8$MNepers/sec. The BOC(1,1) (Galileo Open Service code), gives an error contours comparable to the BOC(0,1). The higher-frequency signals have substantially smaller maximum errors. The ones that have $n>1$, however, show characteristic troughs or peaks around certain intermediate values of $F_d$; the other codes tend to peak only as $F_d$ approaches zero.

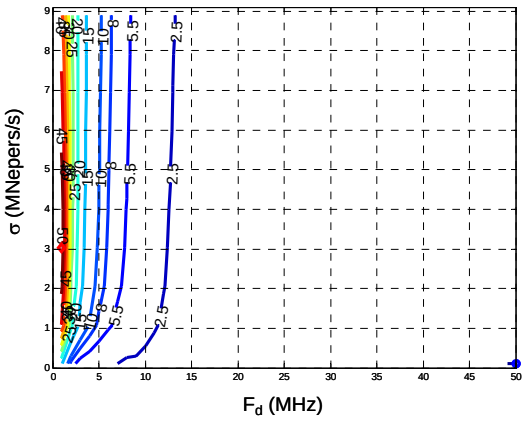


**Fig. 14 BOC(0,1) – Analog failure-induced range biases (meters) for a correlator spacing of 0.05 C/A code chips**

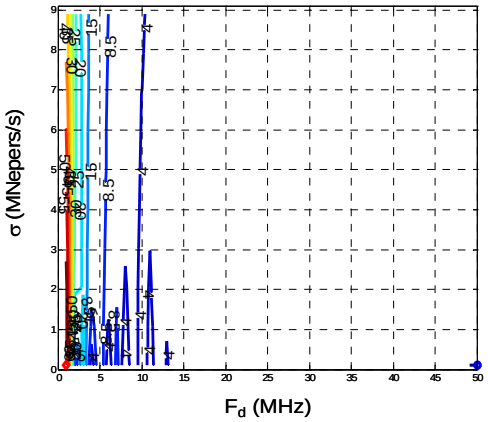


**Fig. 15 BOC(1,1) – Analog failure-induced range biases (meters) for a correlator spacing of 0.05 [BOC(1,1)] code chips**

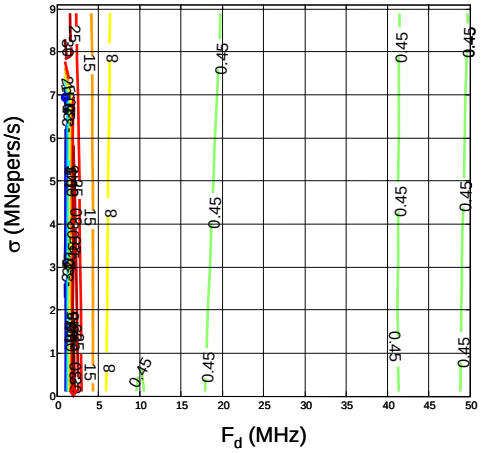


**Fig. 16 BOC(0,10) – Analog failure-induced range biases (meters) for a correlator spacing of 0.5 [BOC(0,10)] code chips**

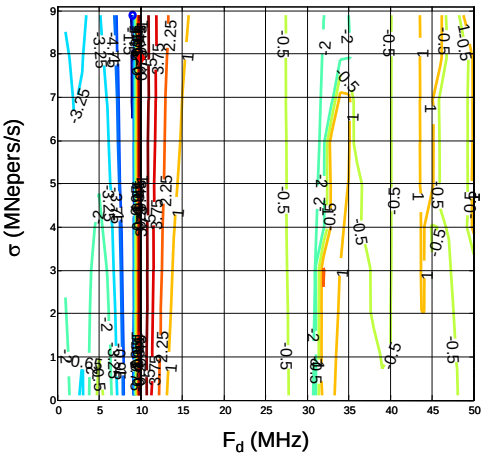


**Fig. 17 BOC(10,5) – Analog failure-induced range biases (meters) for a correlator spacing of 0.25 [BOC(10,5)] code chips**

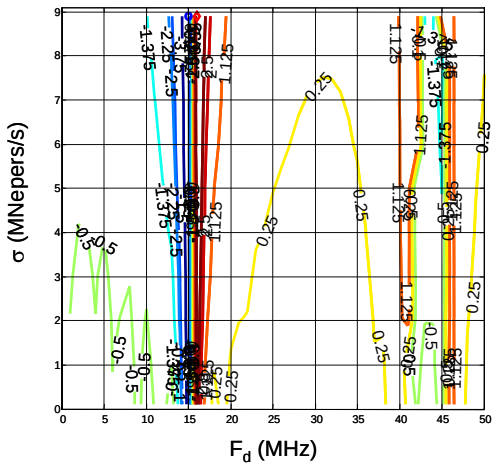


**Fig. 18 BOC(15,2.5) – Analog failure-induced range biases (meters) for a correlator spacing of 0.04 [BOC(15,2.5)] code chips**

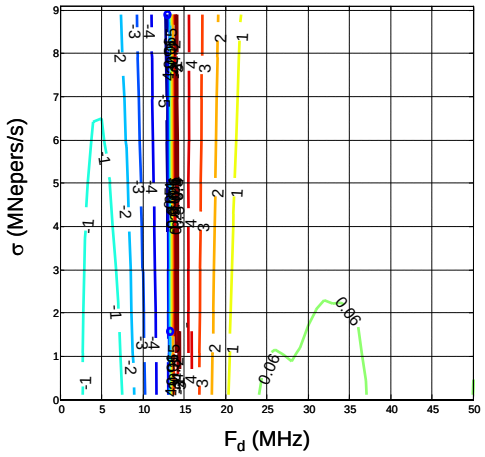


**Fig. 19 BOC(15,10) – Analog failure-induced range biases (meters) for a correlator spacing of 0.2 [BOC(15,10)] code chips**

## 4 Conclusions

The digital and analog failure modes of the ICAO threat model were applied to the ideal, envisioned signals for GPS and Galileo. The errors were shown to vary significantly as a function of early-minus-late correlator spacings and threat model parameters. Higher-frequency modulations seem to decrease the maximum error due to either failure mode; however they tend to introduce some unpredictability with respect to correlator spacing. For high-integrity differential applications such as WAAS and LAAS, these factors should be considered in the selection of a correlator configuration for a reference receiver and in the span of allowable configurations for avionics receivers.

These results demonstrate the need for a precise threat model definition, receiver filter design, and code tracking implementation constraints. However, if these are considered together, it may be possible to envision a differential system that minimizes the impact of these failures in the future.

## References

Brenner M, Kline P, Reuter R, (2002) *Performance of a Prototype Local Area Augmentation System (LAAS) Ground Installation,* Proceedings of the 2002 15th International Technical Meeting of the Satellite Division of the Institute of Navigation, ION GPS/GNSS-2002.

Edgar C, Czopek F, Barker B (2000) *A Co-operative Anomaly Resolution on PRN-19,* Proceedings of the 2000 13th International Technical Meeting of the Satellite Division of the Institute of Navigation, ION GPS-2000. Proceedings of ION GPS 2000, v 2, pp. 2269-271.

Enge P.K., Phelts R. E., Mitelman A. M., (1999) *Detecting Anomalous signals from GPS Satellites,* ICAO, GNSS/P, Toulouse, France.

Mitelman A. M. (2005) *Signal Quality Monitoring For GPS Augmentation Systems,* Ph.D. Thesis, Stanford University, Stanford, CA.

Phelts, R. E. (2001) *Multicorrelator Techniques for Robust Mitigation of Threats to GPS Signal Quality*, Ph.D. Thesis, Stanford University, Stanford, CA.

Phelts R. E., Akos D. M., Enge, P. K. (2000) *Robust Signal Quality Monitoring and Detection of Evil Waveforms,* Proceedings of the 13th International Technical Meeting of the Satellite Division of the Institute of Navigation, ION-GPS-2000, pp. 1180-1190.